Results in Engineering 30 (2026) 110830

Contents lists available at ScienceDirect

Results in Engineering

journal homepage: www.sciencedirect.com/journal/results-in-engineering

Research paper

Non-invasive gesture recognition using PDMS-encapsulated polymer optical fiber Bragg gratings

Yiding Xu [a], Weibin Liang [b], Binbin Luo [a,*], Hang Qu [b], Getinet Woyessa [c], Ole Bang [c], Xuehao Hu [d,*]

[a] Chongqing Key Laboratory of Optical Fiber Sensor and Photoelectric Detection, Chongqing University of Technology, Chongqing 400054, China
[b] Department of Physics, College of Science, Shantou University, Shantou, China
[c] DTU Electro, Department of Electrical and Photonics Engineering, Technical University of Denmark, 2800 Kgs, Lyngby, Denmark
[d] Department of Electromagnetism and Telecommunication, University of Mons, Mons 7000, Belgium

ARTICLE INFO

Keywords:
POFBG
Forearm muscle sensing
Gesture recognition
CNN-LSTM-attention

ABSTRACT

This paper introduces a non-invasive and high-sensitivity method for gesture recognition based on polymer optical fiber Bragg grating (POFBG) sensors embedded in polydimethylsiloxane (PDMS). Experimental results show that PDMS-encapsulated POFBGs exhibit bending sensitivities for finger and wrist motions that are 8.3 times that of conventional silica optical fiber Bragg gratings, while maintaining excellent repeatability. For gesture recognition, four POFBG sensors are strategically attached to specific forearm muscles to monitor muscle deformations produced by various gestures. The response characteristics and sensing performance of the sensors are comprehensively validated. A convolutional neural network–long short-term memory–attention model is employed to train and predict 16 gestures, including five static wrist gestures, eight static finger gestures, and three dynamic gestures. The model effectively discriminates subtle wavelength shifts caused by fine finger movements, achieving an overall recognition accuracy of 95.85% across different subjects. The proposed approach enables integrated and precise recognition of both static and dynamic gestures using a minimal number of sensors, achieving an optimal balance between recognition accuracy, coverage, and device portability. This work provides a high-performance and cost-effective sensing solution for advanced human–computer interaction applications.

1. Introduction

The human hand, as a highly specialized motor organ, exhibits remarkable flexibility and movement precision due to its complex skeletal structure, numerous muscle groups, and sophisticated neural regulation mechanisms [1]. With the rapid development of artificial intelligence, deep learning, and sensor technologies, the accuracy and real-time performance of gesture recognition systems have improved significantly, expanding their potential applications. From smart home control [2] to medical rehabilitation [3,4] and virtual reality [5],gesture recognition has become a key enabler of natural human–computer interaction. Gesture detection methods can be broadly classified into two categories: non-contact sensors and contact sensors. Non-contact sensors, such as those based on visual perception [6], are easily affected by environmental conditions, including lighting and background interference, and often exhibit high power consumption and cost. In contrast, contact sensors are immune to ambient light and color variations. Among contact sensors, those based on electrical signal conversion are widely used [7–9] however, they typically suffer from limitations such as complex fabrication, vulnerability to electromagnetic interference, and relatively high power consumption [10]. Fiber optic sensing technology, with its advantages of excellent immunity to electromagnetic interference, low signal loss, high sensitivity, and wide adaptability [11], offers superior performance in environments where traditional electrical sensors operate unreliably [12]. Consequently, fiber optic sensors have attracted growing attention in the field of wearable sensing.

In hand motion detection, glove-based sensors remain one of the most common solutions. Most fiber optic glove systems adopt one of two major sensing principles: fiber Bragg grating (FBG) wavelength modulation or light intensity modulation. Examples of the former include Jha et al. [13,14], who proposed a high-precision instrumentation glove

* Corresponding authors.
E-mail addresses: luobinbin@cqut.edu.cn (B. Luo), xuehao.hu@umons.ac.be (X. Hu).

https://doi.org/10.1016/j.rineng.2026.110830
Received 25 April 2026; Accepted 30 April 2026
Available online 1 May 2026

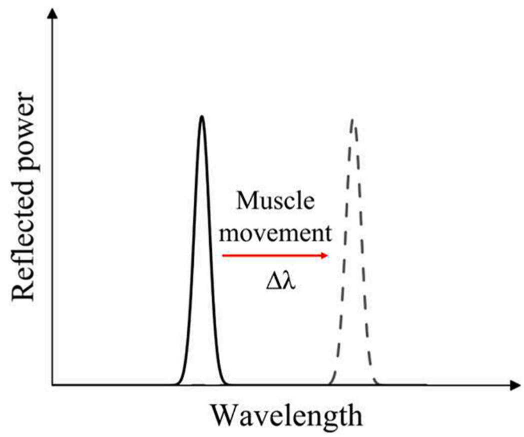

Fig. 1. Schematic diagram of the FBG sensing principle.

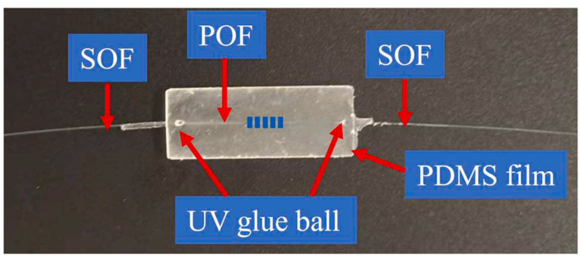

Fig. 2. POFBG sensor encapsulated with PDMS.

with a spring-integrated FBG sensor structure, achieving an average monitoring error of 0.80° across ten thumb joints. Li et al. [15] embedded FBGs into silicone tubes and integrated them into glove joints, successfully distinguishing finger movements. Socorro-Leranoz et al. [16] designed a fiber optic sensing platform based on multiplexed FBGs for detecting finger motions.

For light intensity modulation–based designs, Zha et al. [17] employed flexible polymer optical fiber (POF) sensors for joint movement monitoring, achieving over 90% accuracy. Wang et al. [18] developed an integrated smart glove using POF sensors, while Li et al. [19] proposed a D-shaped POF (D-POF) curvature sensor system that achieved recognition accuracies of 99.8% and 97.7% for 13 gestures and 11 grasping actions, respectively. Although glove-based systems can directly measure joint motion, they typically require multiple sensors, resulting in increased weight, cost, and reduced flexibility of hand movement.

Wristband-based sensors represent another important class of wearable hand-motion detection devices. Zhang et al. [20] designed a sensor based on microfiber evanescent field intensity modulation, achieving a 98.80% recognition accuracy for ten dynamic gestures. Similarly, Wang et al. [21] developed a gesture recognition wristband using micro/nanofibers (MNF) operating under the same principle, with an accuracy of 94%. Liang et al. [22] proposed a wristband-type POF sensor based on POF speckle intensity modulation. Integrated with a smartphone and neural network algorithm, their system achieved a recognition accuracy of 91%. Although wristbands are lighter and more portable than gloves, the signals they capture are often indirect, limiting recognition precision. Furthermore, fixed wristband dimensions make it difficult to accommodate users with different forearm sizes.

With ongoing advancements, researchers have increasingly shifted attention toward forearm muscle–based sensing. Signals obtained by monitoring forearm muscle deformation are more direct and stable, while the sensing device itself is lighter and more comfortable to wear. Guo et al. [23,24] developed an FBG sensor using a polyimide (PI) substrate, in which six sensors connected in series were used to detect deformations caused by forearm muscle contractions, enabling the recognition of six gestures. Yi et al. [25] from our group arranged four FBG sensors based on polydimethylsiloxane-polyimide (PDMS–PI) composite substrates on forearm muscles, achieving a recognition accuracy of 96.67% for eight static gestures across multiple subjects. However, these studies still face several limitations. First, the number of recognizable gestures remains small, restricting practical versatility. Second, most systems focus on either wrist or finger gestures exclusively, and third, static and dynamic gesture recognition are often treated separately rather than in an integrated framework. Therefore, existing approaches require further improvement in comprehensiveness and practical applicability.

Compared with conventional silica optical fiber Bragg gratings (SOFBGs), polymer optical fiber Bragg gratings (POFBGs) retain all the advantages of FBG sensing technology while offering unique material properties, including a Young's modulus more than an order of magnitude lower than that of their silica counterparts, greater flexibility, biocompatibility and resistance to brittleness [26]. These characteristics enable POFBGs to detect subtle strain variations caused by forearm muscle motion with high accuracy. Previous studies have demonstrated that PDMS-encapsulated POFBG sensors can be effectively attached to forearm muscles for physiological monitoring, such as measuring respiratory or heart rates [27].

In related fields (e.g., mechanical fault diagnosis), recent studies have proposed advanced strategies for dynamic signal analysis, including phase entropy-based feature extraction [28], multi-scale feature fusion [29], and multi-sensor information integration [30]. These methods can address challenges such as few-shot learning and motion variability, yet they have not been adapted to wearable gesture recognition systems based on POFBG sensors, thus providing critical methodological references for this study.

To address the limitations of existing gesture recognition systems, including limited gesture coverage, separate recognition of static and dynamic gestures, and the trade-off between portability and accuracy, this study aims to develop a comprehensive, high-performance non-invasive sensing solution. Specifically, a PDMS-encapsulated POFBG sensor array is designed for forearm muscle sensing, leveraging the material advantages of POFBGs to enhance sensitivity to finger and wrist movements. Subsequently, integrated recognition of static and dynamic gestures is achieved, covering a diverse set of hand motions including wrist gestures, finger gestures, and complex dynamic gestures. Finally, a deep learning model is proposed, which enables the proposed solution to maintain high recognition accuracy for multi-type gestures.

2. Principle of operation

The core operating principle of POFBGs is based on the selective reflection of specific wavelengths by the grating structure. Only the wavelength (λ_B) that satisfies the Bragg condition is strongly reflected, while all other wavelengths are almost completely transmitted. The central wavelength of the reflected narrowband spectrum can be expressed as:

$$\lambda_B = 2n_{eff}\Lambda \tag{1}$$

where λ_B is the Bragg wavelength, n_{eff} is the effective refractive index of the fundamental mode, and Λ is the grating period. Variations in n_{eff} and Λ, caused by temperature or axial strain, result in shifts of λ_B.

The experiments were conducted in a constant-temperature environment, with the sensors securely attached to the subject's forearm skin. Since the temperature of the human forearm remains relatively stable, thermal effects on the sensors can be neglected. Under these conditions, the wavelength shift of the FBG can be attributed solely to axial strain and is described by [24]:

$$\Delta\lambda_B/\lambda_B = (1 - P_e)\Delta\varepsilon \tag{2}$$

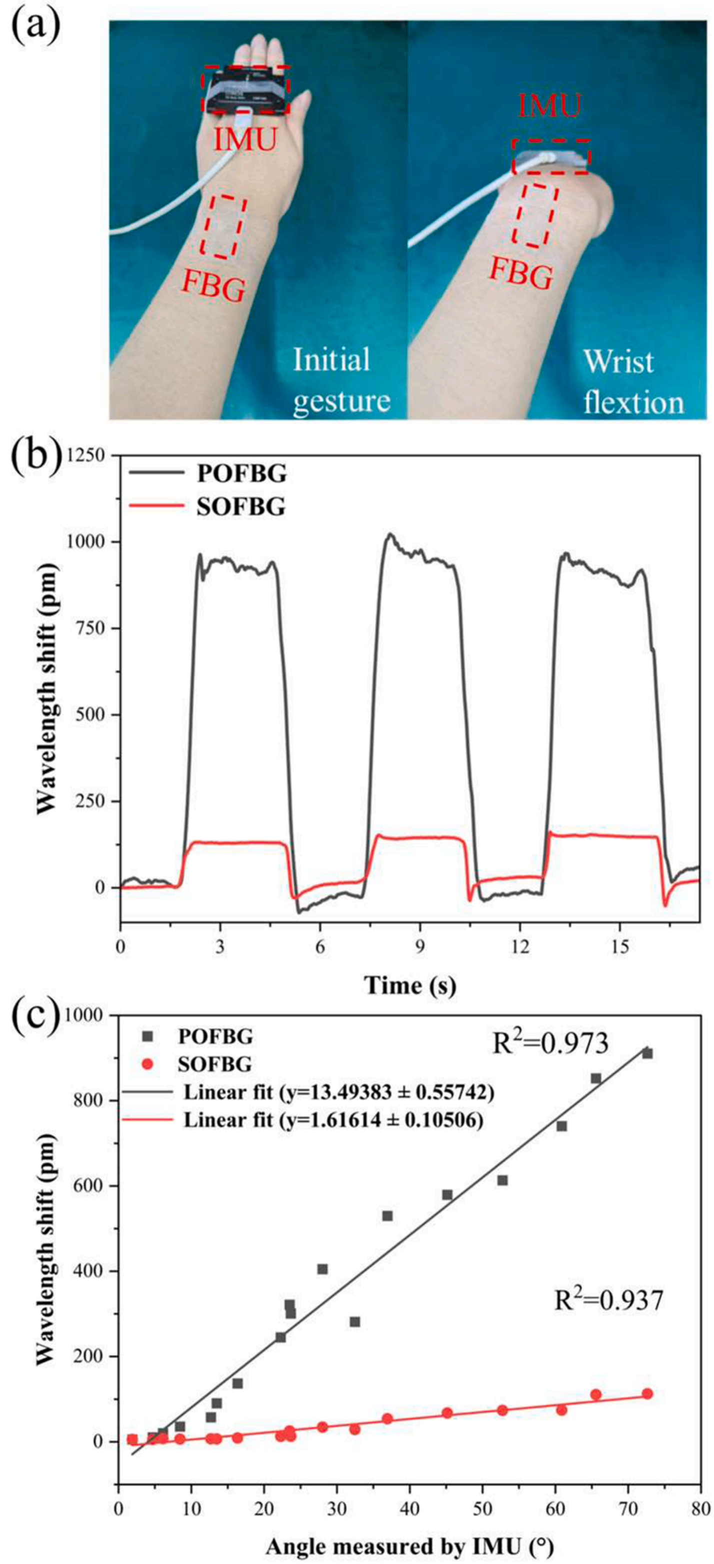

Fig. 3. (a) Wrist flexion–extension movements and sensor placement positions. (b) Comparison of wavelength shifts between SOFBG and POFBG during wrist flexion. (c) Fitted curve of wrist bending sensitivity for the two types of sen-sors.

where P_e is the photoelastic coefficient of the fiber core and $\Delta\varepsilon$ represents the variation in axial strain.

When FBGs are employed to monitor forearm deformation, each gesture induces distinct muscle movements that generate localized strain variations. As the forearm deforms, the resulting strain causes corresponding wavelength shifts in the FBG signals, as illustrated in Fig. 1. Gesture recognition can thus be achieved by analyzing these wavelength shift patterns.

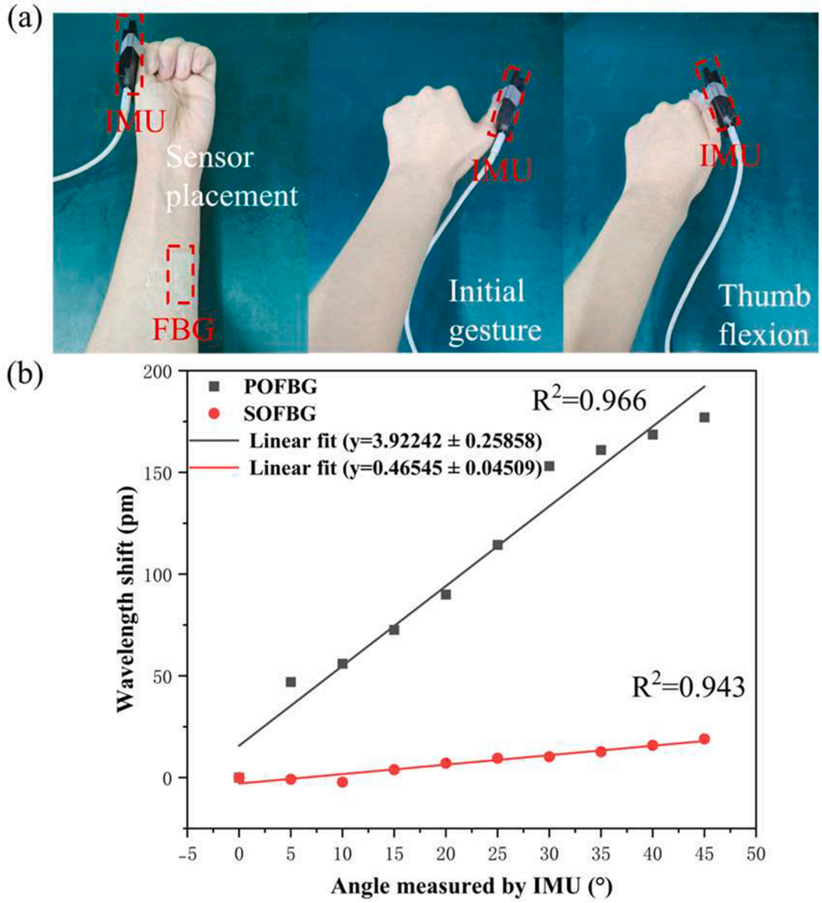

Fig. 4. (a) Thumb bending movement and sensor placement positions. (b) Fitted curve of finger bending sensitivity for the two types of sensors.

Table 1
Muscles and their corresponding sensors.

Muscle	Corresponding sensor
Extensor indicis	FBG1
Extensor digiti minimi	FBG2
Flexor digitorum superficialis	FBG3
Extensor digitorum	FBG4

3. Sensor design and fabrication

3.1. POFBG sensor fabrication

To comprehensively detect forearm muscle deformation, the sensor must possess sufficient flexibility to conform closely to human skin, thereby achieving high sensitivity to subtle muscular movements. Compared with the widely used SOFBGs [31], this study employs POFBGs for forearm muscle monitoring. An optical fiber grating interrogator (GC-97001C-02–02-A-F, Zhuhai Guangchen Technology Co., Ltd.) operating over a wavelength range of 1525–1565 nm, with a sampling rate of 1 kHz and a wavelength accuracy of 2 pm, was employed to demodulate the Bragg wavelength signals from the FBG sensors.

The polymer gratings used in this work were inscribed in a POF composed of TOPAS (5013S-04, TOPAS Advanced Polymers) as the core and ZEONEX (480R, ZEON CORPORATION) as the cladding [32]. The POF was connected to the silica optical fiber (SOF) using UV-curable (Norland 86H) adhesive with an appropriately matched refractive index to ensure low-loss coupling. Subsequently, the POFBGs were fabricated using a 520 nm femtosecond laser via point-by-point inscription technology [33], and the length of each grating was 3 mm. Owing to the low Young's modulus and high flexibility of POFs, the sensors exhibited accurate signal capture, stable optical transmission, and excellent structural reliability.

The fabricated sensors were encapsulated in PDMS [34] to enhance their flexibility and biocompatibility. To improve the adhesion of the encapsulant, the PDMS mixture (Dow Corning, Sylgard 184) was prepared with a ratio of 1.0 mL silicone gel: 0.11 mL curing agent: 2.1 μL ethoxylated polyethylenimine (PEIE). The mixture was cured in an oven at 60 °C for 8 h. The final sensor dimensions were 30 mm × 15 mm × 1 mm, optimized for ergonomic conformity to the forearm surface. The inclusion of PEIE significantly increased the adhesion of PDMS compared with conventionally cured formulations, thereby enhancing bonding between the sensor and the skin [27]. At the same time, the compliance and elongation at break of PDMS were also improved. The PDMS-encapsulated POFBG sensor is illustrated in Fig. 2.

3.2. POFBG sensor characteristics

To verify the static load stability of the sensor, a constant force of 1 N was applied to the encapsulated POFBG sensor for 3 min. The results show that the sensor responds rapidly with no obvious delayed drift, and the output is stable with minimal creep. The wavelength fluctuation is within 1.3 pm, accounting for only 1.45% of the full scale, confirming its excellent creep resistance and static stability. Given that static gestures in wearable applications typically last only a few seconds, the 3-minute test is sufficient to validate the long-term stability for the target scenario.

To achieve more effective monitoring of forearm muscle deformation, the sensor must exhibit high sensitivity to hand movements. A

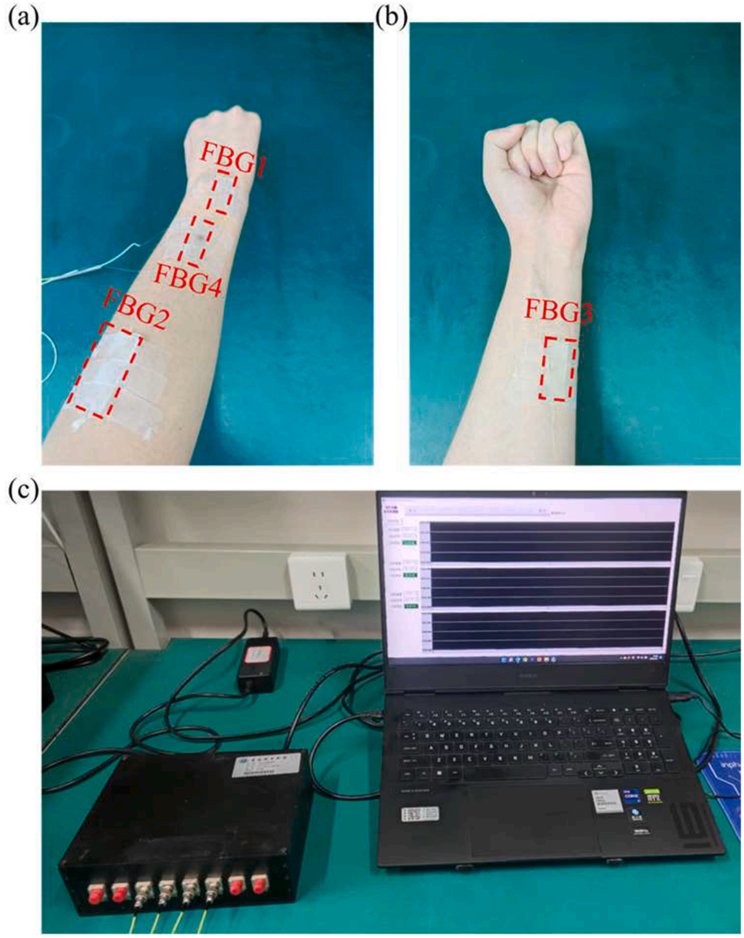

Fig. 5. Actual layout photograph of the sensors on the forearm: (a) back side and (b) front side. (c) experimental setup showing the connection between the POFBG sensors, optical fiber demodulator, and data acquisition computer.

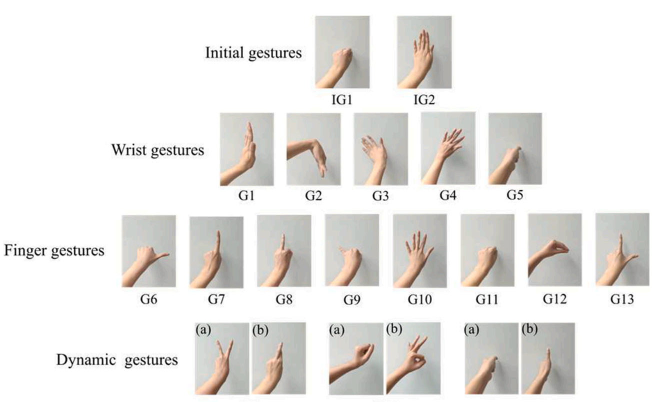

Fig. 6. Schematic diagrams of the two initial gestures and sixteen test gestures.

comparative experiment was conducted between POFBGs encapsulated in PDMS and conventional SOFBGs. The sensors were positioned on the extensor indicis muscle, while inertial measurement unit (IMU) sensors were mounted on the four fingers, excluding the thumb, to synchronously collect angular velocity and acceleration data for calibrating wrist bending angles and motion amplitudes,as illustrated in Fig. 3(a).

During the experiment, wrist flexion–extension movements were performed in cycles: the initial position was maintained for 2 s, followed by 3 s of wrist flexion–extension, and this sequence was repeated three times. The corresponding experimental results are shown in Fig. 3(b).

On average, the response and recovery times of the POFBG were 530 ms and 740 ms, slower than the SOFBG's 310 ms and 250 ms. However, this time difference is far smaller than the duration of static and dynamic gestures. The system cap-tures full temporal features rather than instantaneous samples, and the sensor stabilizes fully before gesture completion, so real time recognition is unaffected. Meanwhile, the POFBG's wavelength shift (940 pm) is much larger than the SOFBG's (122 pm), significantly enhancing signal to noise ratio and feature distinguishability. It clearly captures subtle muscle deformations in dynamic gestures, facilitating feature extrac-tion and recognition, effectively compensating for the time difference and ensuring recognition accuracy and stability.For the first sequence, the wavelength shifts as a function of movement angle are shown in Fig. 3(c). The bending sensitivity of the SOFBG to wrist motion was approximately 1.61 pm/°, whereas that of the POFBG was about 13.49 pm/°, which is roughly 8.4 times that of the SOFBG.

To investigate the relationship between wavelength shift and finger movement angle during gesture execution, the sensors were placed on the flexor digitorum superficialis muscle, while an IMU sensor was attached to the thumb, as shown in Fig. 4(a). The thumb was bent at a constant speed. The wavelength shifts as a function of movement angle are presented in Fig. 4(b).

The bending sensitivity of the SOFBG for finger movements was approximately 0.47 pm/°, whereas that of the POFBG was about 3.92 pm/°, approximately 8.3 times that of the SOFBG. This indicates that even when the sensors are attached to different muscles, the POFBG maintains significantly higher bending sensitivity—whether in finger or wrist movement detection—meeting the experimental requirements for

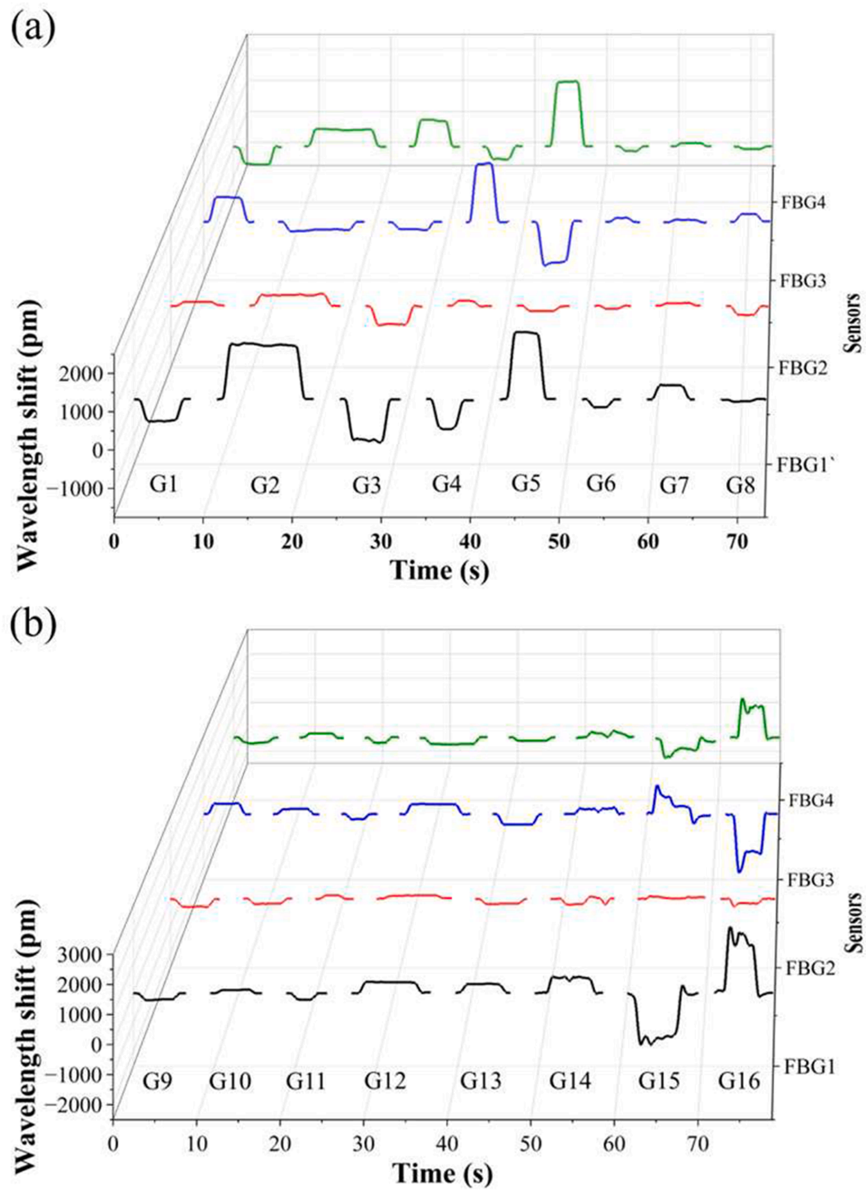

Fig. 7. Three-dimensional visualization of wavelength shifts for the sixteen test gestures: (a) G1–G8 and (b) G9–G16.

high responsiveness and precision.

4. Gesture recognition

4.1. Sensor placement and POFBG array layout

The number and placement of sensors are critical for accurately capturing gesture-related signals. Considering the primary muscles involved in finger extension and flexion, a total of four POFBG sensors were employed. These sensors were positioned on the extensor indicis, extensor digitorum, flexor digitorum superficialis, and extensor digiti minimi muscles, as summarized in Table 1.

Specifically, the extensor digitorum drives the extension of the four fingers and coordinates with wrist extension to open the palm. The flexor digitorum superficialis governs finger flexion and cooperates with wrist flexion to enhance grip stability. The extensor indicis enables independent extension of the index finger and assists with fine wrist adjustments during delicate movements, while the extensor digiti minimi controls independent extension of the little finger and works in conjunction with ulnar wrist deviation to achieve specific postures.

These four muscles perform distinct yet coordinated functions, allowing precise capture of motion-related information. During sensor attachment, each sensor should be aligned with the longitudinal direction of its target muscle to ensure optimal strain sensitivity. Owing to the strong adhesiveness of PDMS, the sensors can be directly affixed to the forearm muscles or additionally secured with medical tape for enhanced stability. The actual sensor placement configuration is shown in Fig. 5. During the experiment, the other end of each sensor is connected to the optical fiber demodulator via optical fiber jumpers, and the demodulator is connected to a computer. The wavelength shift data is monitored and recorded in real time through the host computer software, as illustrated in Fig. 5(c).

4.2. Gesture set and data acquisition

Based on the sensor placement scheme, two types of initial gestures (IG1 and IG2) and sixteen test gestures were designed to comprehensively evaluate the sensor system’s ability to recognize various hand movements. During the experiment, each motion sequence began from an initial gesture, transitioned to the corresponding test gesture, and

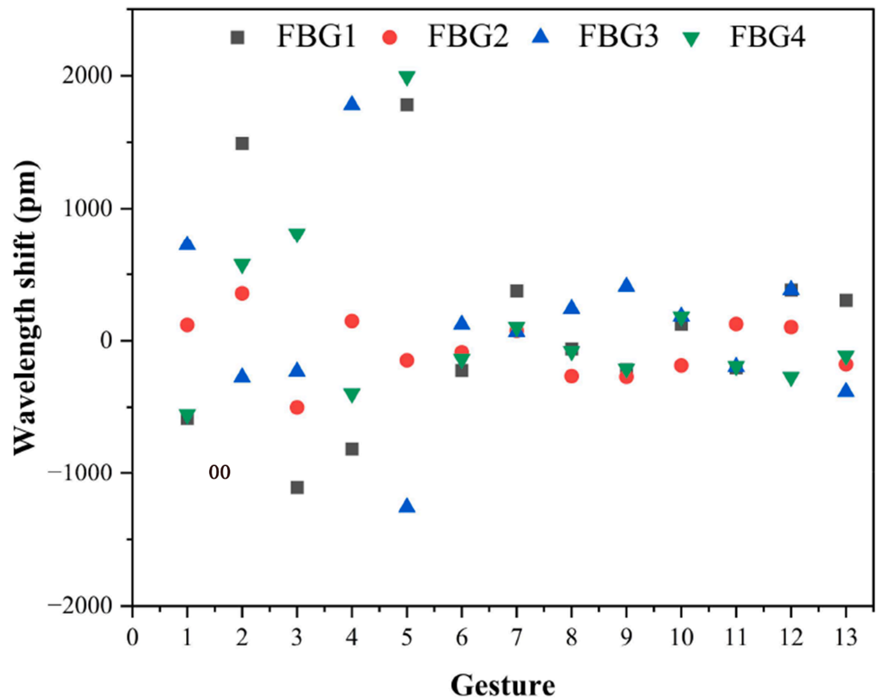

Fig. 8. Average wavelength shifts in the characteristic interval of static gestures.

Table 2
RSD of thirteen static gestures.

Gesture	FBG1	FBG2	FBG3	FBG4	Average
1	2.53%	8.77%	2.6%	3.48%	4.35%
2	2.39%	7.12%	5.91%	4.33%	4.94%
3	1.90%	4.31%	3.79%	4.53%	3.63%
4	2.98%	8.33%	3.88%	4.71%	4.98%
5	2.24%	4.04%	5.48%	4.13%	3.97%
6	4.00%	4.72%	5.48%	4.51%	4.68%
7	1.31%	7.54%	5.25%	4.23%	4.58%
8	7.41%	3.20%	3.29%	4.84%	4.68%
9	4.27%	5.05%	2.06%	7.06%	4.61%
10	7.21%	2.16%	4.85%	4.31%	4.63%
11	3.99%	7.13%	2.97%	4.29%	4.60%
12	2.20%	6.59%	1.61%	2.98%	3.35%
13	2.78%	3.59%	3.16%	6.46%	4.00%

then returned to the initial gesture after maintaining the test position.

Specifically, IG1 corresponded to G5 (wrist rotation), G6 (thumb extension), G7 (index finger extension), G8 (middle finger extension), G9 (little finger extension), G10 (hand opening), G12 (number “7″ gesture), G13 (number “8” gesture), G14 (blessing gesture), G15 (OK gesture), and G16 (encouragement gesture). IG2 corresponded to G1 (wrist extension), G2 (wrist flexion), G3 (wrist ulnar deviation), G4 (wrist radial deviation), and G11 (fist making). Among the sixteen test gestures, Gestures 1–5 represent wrist movements, Gestures 6–13 correspond to finger movements, and Gestures 14–16 are complex dynamic gestures involving both fingers and wrists, as illustrated in Fig. 6.

The wavelength shift corresponding to each gesture was measured using an optical fiber demodulator. Before formal testing, participants were given sufficient practice time to familiarize themselves with the gesture sequence. After confirming their familiarity with the testing procedure, the formal experiments commenced, and the sensor outputs were recorded.

To better simulate real-world conditions, the duration of each gesture was not fixed. Each subject began from the initial posture, maintained it for 1–2 s, transitioned to the target posture, held it for 3–9 s, and finally returned to the initial position. During this process, the sensor output signals were susceptible to external disturbances and noise; therefore, filtering of the acquired wavelength curves was necessary to minimize interference.

For static gesture testing, the signals collected by the fiber optic sensors were relatively stable. The primary objective was to remove noise while maintaining a consistent base-line without excessively smoothing out subtle static feature variations. Accordingly, the Adjacent Averaging method was applied: we set a sliding window size of 5 data points (corresponding to a 5 ms time window, matching the 1 kHz sampling rate of the interrogator), enabled the "Central Point" mode (replacing the window’s central data point with the arithmetic mean of 5 consecutive wavelength shift data points), and applied the filter across the entire signal se-quence.

For dynamic gesture testing, the goal was to suppress noise while preserving the overall dynamic trends and key inflection points of the motion signals; thus, the Savitzky–Golay filtering method was employed for smoothing. The parameters were configured as follows: a polynomial order of 2 (to avoid overfitting), a sliding window size of 11 data points (11 ms time window), and the default "No Deriva-tive" mode, which fits local data points with a low-order polynomial to retain motion-related features.The processed wavelength shift curves for all sixteen gestures obtained from the experiments are shown in Fig. 7.

4.3. Static gesture analysis and repeatability

To facilitate the analysis of the thirteen static gestures, each gesture was repeated five times consecutively. Fig. 8 presents the average wavelength shifts within the characteristic interval across multiple static gesture experiments.

Because wrist movements involve larger motion amplitudes than finger gestures, the sensors experience greater strain due to muscle stretching. Consequently, the wavelength shifts of G 1–G5 (wrist movements) are significantly larger than those of G6–G13 (finger movements). Taking G1 as an example, FBG2 and FBG3 exhibit red shifts, while FBG1 and FBG4 show blue shifts. In contrast, for G2, only FBG3 experiences a blue shift, with FBG1, FBG2, and FBG4 all displaying red shifts. This distinct difference in wavelength shift patterns allows these two wrist gestures to be clearly distinguished.

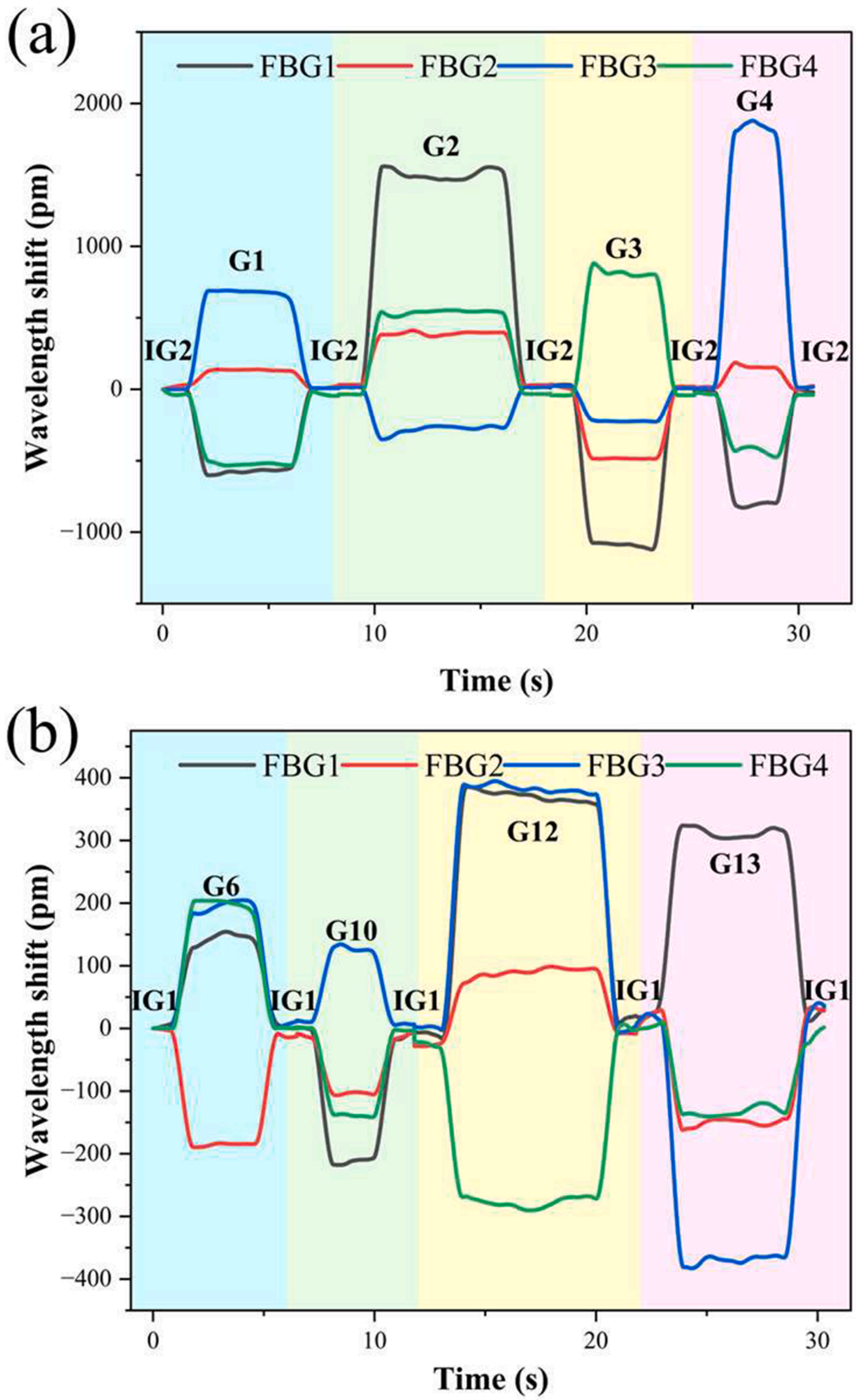

Fig. 9. Wavelength shift diagrams during continuous execution of different gestures: (a) successive wrist motions and (b) successive finger motions.

A similar analysis of G4 shows that its four sensors exhibit a wavelength shift trend similar to that of G1. However, differences in wrist motion amplitude and muscle contraction intensity between these gestures lead to varying degrees of muscle strain, resulting in noticeable differences in the magnitude of wavelength shifts. Therefore, static gesture recognition can be effectively achieved by leveraging both the distinct wavelength shift patterns across different sensors and the magnitude variations of these shifts under similar strain trends.

Due to variations in wavelength shift magnitudes among sensors, the relative standard deviation (RSD) was employed to evaluate the repeatability of the sensor output signals. The corresponding data are presented in Table 2. In this study, four POFBG sensors were used to construct a distributed sensing network. Gesture recognition in this configuration does not depend on the absolute repeatability of any single sensor; instead, the multi-sensor arrangement provides feature redundancy and complementarity from a spatial perspective.

Although the maximum RSD value of an individual sensor reached 8.77%, mainly due to its location over narrow or mechanically complex muscle regions where slight involuntary co-contraction and micro-displacement introduce signal variability, the maximum average RSD

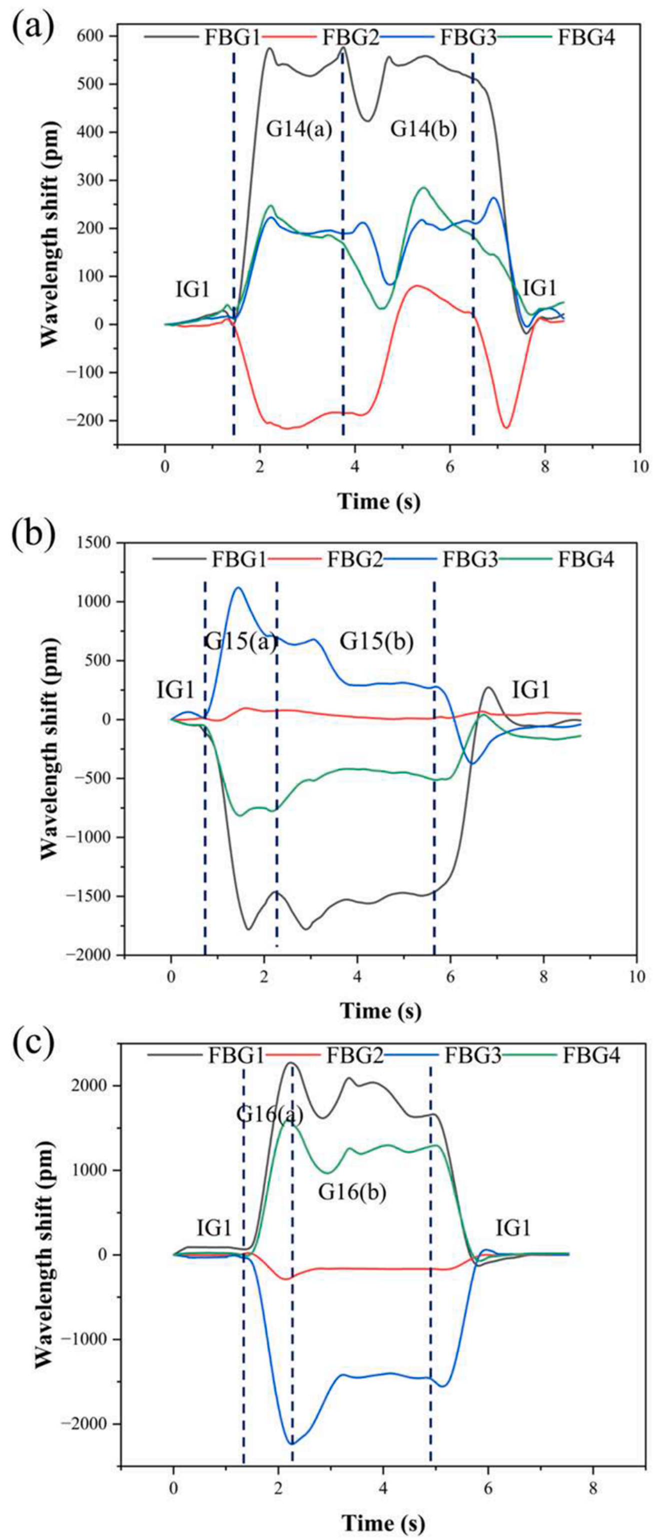

Fig. 10. Wavelength drift curve diagrams of three dynamic gestures: (a) G14. (b) G15, (c) G16.

value across the thirteen gesture types was only 4.98%. These results demonstrate that after multi-sensor signal fusion, the dispersion in the output signals remains well controlled, indicating excellent system stability.

The wavelength shift curves recorded during transitions between different gestures are shown in Fig. 9. Even during gesture switching, the static characteristics of the signals remain consistent, further verifying the reliability of the sensor system in capturing stable and repeatable gesture-related strain information.

For the three dynamic gestures selected from the tested set (Fig. 10), recognition primarily depends on analyzing the changes in wavelength shift magnitude and the overall trend of the signal during gesture transitions.

Taking G16 as an example, during the first half of its execution, the movement resembles a rotational motion; consequently, the wavelength curve exhibits a pattern similar to that of rotational gestures. In the subsequent phase, the action of raising the thumb induces a distinct change in the wavelength shift, which is clearly reflected in the signal curve. A similar phenomenon is observed during the execution of G14 and G15, where sudden wavelength variations occur at specific motion phases.

By leveraging these “sudden-shift” features, namely the abrupt wavelength-drift variations manifested as distinct redshift or blueshift trends induced by rapid hand movements that directly reflect gesture initiation, direction, and transient characteristics, together with the overall variation trends of the wavelength curves throughout gesture execution, dynamic gestures can be effectively recognized.This confirms that the POFBG sensor system, combined with targeted signal analysis, can accurately capture transient strain variations caused by dynamic hand movements, thereby distinguishing different types of dynamic gestures.

5. Gesture recognition by deep learning

The collected data were processed and classified using a CNN–LSTM–Attention hybrid algorithm, whose network architecture is illustrated in Fig. 11. The input is a sequence with a fixed length of 128 time steps and 4 POFBG channels, resulting in an input shape of [batch_size, time_steps, channel] (i.e., (32, 128, 4)) — where 32 corresponds to the batch size used in training.The wavelength shift data were Min–Max normalized to the range [0, 1] and further standardized within each sample, while Gaussian noise with a level of 0.01 was added for data augmentation.A two-layer 1D CNN (with channel dimensions 4→64→64, 3×1 convolution kernels, and padding=1), integrated with batch normalization, ReLU activation, and a dropout rate of 0.1, was employed to extract local spatial features. A single-layer bidirectional LSTM (with a hidden size of 128) captured temporal dependencies, and an additive attention module adaptively weighted key temporal segments. Finally, a fully connected layer mapped the aggregated features to 16 gesture categories.The model was trained using the Adam optimizer (learning rate = 1e-4) and cross-entropy loss, with a batch size of 32 and 500 training epochs. The entire training process was completed within several minutes on a workstation equipped with an AMD Ryzen 7 7735H CPU and an NVIDIA GeForce RTX 4060 GPU. The average inference time for a single sample is <5 ms on the test GPU, ensuring the system meets the response requirements for natural, moderate-speed gesture interaction.

A total of five subjects (three males and two females, covering both slim and robust builds) participated in the experiments, producing over 2000 gesture samples for deep learning. Of these, 80% were used for training and 20% for testing. The long short-term memory (LSTM) algorithm, commonly applied in gesture recognition, achieved an overall recognition accuracy of 90.93% for sixteen gestures. In contrast, the proposed CNN–LSTM–Attention model integrated local spatial features with the temporal weighting of key time segments, significantly improving classification performance.

The training results are presented in Fig. 12, where the recognition accuracy for static gestures reaches 95.29%, that for dynamic gestures stands at 97.75%, and the overall recognition accuracy for all 16 gestures is 95.85%. Meanwhile, the model is capable of maintaining stable recognition accuracy, and the core factor influencing the system performance lies in whether the sensors can be accurately placed on the corresponding muscles, rather than the passage of time.

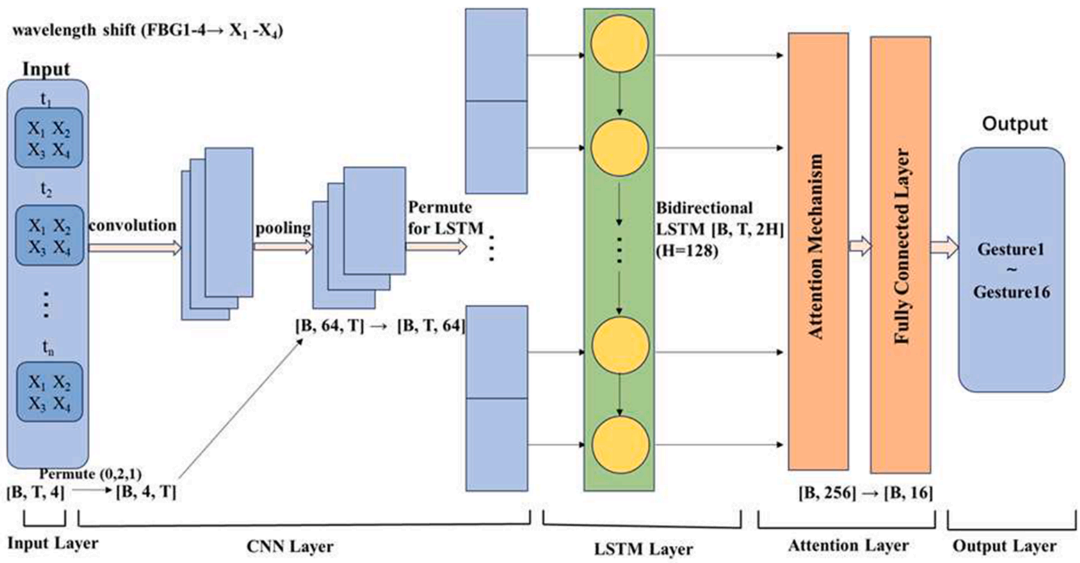

Fig. 11. Architecture diagram of the CNN–LSTM–Attention network.

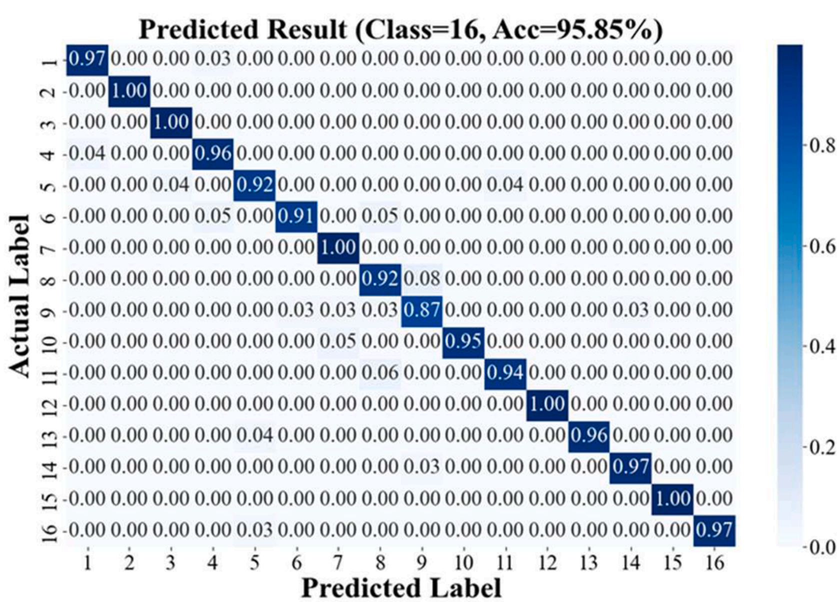

Fig. 12. Gesture recognition performance of the sixteen gestures using the CNN–LSTM–Attention algorithm.

Table 3
Comparison of gesture recognition research results.

Sensor	Placement	Gesture	Sensor Count	Quantity	Dynamic	Algorithm	Accuracy
POF [18]	Finger	Finger	5	16	No	Random forest	98.4%
D-POF [19]	Finger	Finger	5	13	No	SVM	99.8%
MNF [21]	Wrist	Finger	3	12	No	SVM	94%
POF [22]	Wrist	Finger	1	10	No	SAD	91%
FBG [25]	Forearm muscles	Finger+Wrist	4	8	No	LSTM	96.67%
sEMG [35]	Forearm muscles	Finger+Wrist	8	5	yes	CNN-LSTM	84.2%
Mult-sensor [36]	Finger	Finger+Wrist	11	5	yes	CNN	90%
POFBG (this work)	Forearm muscles	Finger+Wrist	4	16	yes	CNN-LSTM-attention	95.85%

SVM: support vector machine.
SAD: sum of absolute differences.
sEMG: surface electromyographic.

Misclassifications mainly occur in gestures with highly similar muscle activation patterns (e.g., G5, G6, G9), owing to the overlapping strain responses captured by the fiber Bragg grating (FBG) sensors. Future research will focus on optimizing the sensor placement scheme and introducing a multi-modal sensing technique to better distinguish the subtle differences between similar gestures.

6. Discussion

To clarify the performance of the proposed method, Table 3 presents a parameter-by-parameter comparison between this study and previous works based on sensor attributes.

Glove-type sensors [18] and [19], despite achieving high recognition accuracies of 98.4% and 99.8% respectively, rely on a relatively large number of sensors (5 sensors each) and are limited to recognizing only static finger gestures, lacking support for dynamic gesture recognition. Wristband-type sensors [21] and [22] can only identify static finger gestures, and their recognition performance is relatively poor, with accuracies of 94% and 91% respectively.The FBG-based study [25], with sensors deployed on the forearm muscles, targets wrist movements and achieves an accuracy of 96.67% while supporting only 8 static gesture categories.Other sensing approaches [35] and [36] use a large number of sensors (8 and 11 sensors, respectively) to perform dynamic gesture recognition that combines finger and wrist movements. However, they only support a small number of identifiable gestures (5 categories) and achieve relatively low accuracies (84.2%–90%), resulting in modest overall performance.

In contrast, the POFBG-based system proposed in this work—implemented on forearm muscles with only 4 sensors—exhibits excellent performance across all evaluation parameters. It provides a more comfortable wearing experience compared with glove- and wristband-type devices. In terms of gesture coverage, it recognizes 13 static gestures (integrating both finger and wrist categories, overcoming the limitation of single-type recognition) and 3 dynamic gestures (addressing the absence of dynamic gesture recognition in prior studies). In terms of accuracy, the system achieves a high overall recognition rate of 95.85% through the CNN–LSTM–Attention mechanism.

By balancing multi-type static gesture coverage and dynamic gesture recognition, the proposed system achieves superior comprehensive performance, demonstrating both high recognition precision and excellent adaptability compared with previously reported methods.

7. Conclusion

This study presents a gesture recognition method based on monitoring forearm muscle deformation using POFBGs. Four sensors were strategically placed on the extensor indicis, extensor digitorum, flexor digitorum superficialis, and extensor digiti minimi muscles to enable non-invasive detection of finger and wrist movements.

Experimental results confirmed that the PDMS-encapsulated POFBGs exhibited excellent creep resistance, high flexibility, and significantly enhanced sensitivity compared with conventional SOFBGs, which addresses the fragility and low sensitivity limitations of traditional optical fiber sensors in wearable gesture sensing. Using this sensing system, thirteen static gestures and three dynamic gestures were successfully recognized, with a maximum average RSD of only 4.98%, demonstrating strong signal stability and repeatability. Notably, the low RSD value indicates that the system can maintain consistent performance across multiple measurements, which is critical for practical long-term use.

A dataset collected from five subjects was used to train the CNN–LSTM–Attention model, which achieved recognition accuracies of 95.29% for static gestures, 97.75% for dynamic gestures, and an overall accuracy of 95.85%. This high recognition performance validates the effectiveness of the proposed hybrid network in fusing spatial-temporal features for complex gesture classification. The proposed system provides a lightweight, flexible, and electromagnetically immune alternative to glove- or wristband-based devices, showing strong potential for practical applications in human–computer interaction.

Despite these promising results, some limitations remain. Variations in individual forearm muscle distribution and strength may affect optimal sensor placement and recognition accuracy, while environmental changes such as temperature fluctuations and humidity could influence sensing performance. These factors restrict the system's generalization ability across diverse user groups and complex real-world environments. To mitigate these effects, PDMS encapsulation is adopted to reduce the direct impact of humidity and perspiration, and skin adhesion is optimized to maintain stable contact. Additionally, the current response time of 530 ms and recovery time of 740 ms may impose limitations for high-speed human–computer interaction (HCI) applications requiring sub-100 ms response. Future research will focus on four specific directions: (1) developing adaptive sensor calibration algorithms to reduce the impact of individual and environmental differences on sensing reliability; (2) integrating real-time temperature compensation algorithms based on the thermo-optic and elasto-optic coefficients of POF to decouple temperature- and strain-induced wavelength shifts; (3) exploring effective technical approaches to reduce the sensor's response latency and improve its dynamic performance to meet the application requirements of more demanding scenarios; (4) extending the system's integration into real-world human–computer interaction scenarios to further enhance its practicality.

CRediT authorship contribution statement

Yiding Xu: Data curation, Formal analysis, Investigation, Software, Visualization, Writing – original draft. **Weibin Liang:** Formal analysis, Methodology, Resources, Validation. **Binbin Luo:** Formal analysis, Funding acquisition, Methodology, Project administration, Supervision, Writing – review & editing. **Hang Qu:** Methodology, Resources, Supervision, Writing – review & editing. **Getinet Woyessa:** Formal analysis, Supervision, Writing – review & editing. **Ole Bang:** Resources, Supervision, Writing – review & editing. **Xuehao Hu:** Formal analysis, Investigation, Methodology, Supervision, Validation, Writing – review & editing.

Declaration of competing interest

The authors declare that they have no known competing financialinterests or personal relationships that could have appeared to influencethe work reported in this paper.

Acknowledgments

The work presented in this article is funded by the National Natural Science Foundation of China (62475140), Chongqing Natural Science Fund Innovation and Development Joint fund (CSTB2023NSCQ-LZX0008), Chongqing University of Technology Research and Innovation Team Cultivation Program (2023TDZ002), Guangxi Key laboratory of Optoelectronic Information Processing (GD23203), The Fonds de la Recherche Scientifique (F.R.S.-FNRS) under the Postdoctoral Researcher grant (Chargé de Recherches) of Xuehao Hu.

Data availability

Data will be made available on request.

References

[1] H. Van Duinen, S.C. Gandevia, Constraints for control of the human hand, J. Physiol. 589 (23) (2011) 5583–5593, https://doi.org/10.1113/jphysiol.2011.217810.

[2] H. Rustam, M. Muneeb, S.A. Alsuhibany, et al., Home automation-based health assessment along gesture recognition via inertial sensors, CMC-Comput. Mater. Con. 75 (1) (2023) 2331–2346, https://doi.org/10.32604/cmc.2023.028712.

[3] L.A. Ngiejungbwen, H. Hamdaoui, M. Chen, Polymer optical fiber and fiber Bragg grating sensors for biomedical engineering applications:a comprehensive review, Opt. Laser. Technol. 170 (2024) 110187, https://doi.org/10.1016/j.optlastec.2023.110187.
[4] P. Lei, Y. Bao, L. Gao, et al., Bioinspired integrated multidimensional sensor for adaptive grasping by robotic hands and physical movement guidance, Adv. Funct. Mater. 34 (26) (2024) 2313787, https://doi.org/10.1002/adfm.202313787.
[5] T. Di Qi, F.L. Cibrian, M. Raswan, et al., Toward intuitive 3D interactions in Virtual reality: a deep learning-based dual-hand gesture recognition approach, IEEE Access. 12 (2024) 67438–67452, https://doi.org/10.1109/ACCESS.2024.3400295.
[6] D. Sarma, M.K. Bhuyan, Methods, databases and recent advancement of vision based hand gesture recognition for HCI systems: a review, SN. Comput. Sci. 2 (6) (2021) 436, https://doi.org/10.1007/s42979-021-00827-x.
[7] K.R. Pyun, et al., Machine-learned wearable sensors for real-time hand-motion recognition: toward practical applications, Natl. Sci. Rev. 11 (2) (2024) 231–263, https://doi.org/10.1093/nsr/nwad298.
[8] M.A. Ozdemir, D.H. Kisa, O. Guren, A. Onan, A. Akan, EMG based hand gesture recognition using Deep Learning. 2020 Medical Technologies Congress, TIPTEKNO, Antalya, Turkey, 2020, pp. 7–19, https://doi.org/10.29081/jesr.v29i2.001.
[9] A. Jaramillo-Yanez, M.E. Benalcazar, E. Mena-Maldonado, Real-time hand gesture recognition using surface electromyography and machine learning: a systematic literature review, Sensors 20 (9) (2020) 2467, https://doi.org/10.3390/s20092467.
[10] J. Chen, Y. Zhou, X. Chen, et al., Recent progress in essential functions of soft electronic skin, Adv. Funct. Mater. 31 (42) (2021), https://doi.org/10.1002/adfm.202104686.
[11] H. Rao, B. Luo, D. Wu, et al., Study on the design and performance of a glove based on the FBG array for hand posture sensing, Sensors 23 (20) (2023) 8495, https://doi.org/10.3390/s23208495.
[12] C. Zhang, H. Zhou, H. Nong, et al., FBG-SenseGlove: a digital twin data glove for underwater gesture recognition using deep learning, IEEE Sens. J. 25 (5) (2025) 8347–8354, https://doi.org/10.1109/JSEN.2025.3532601.
[13] C.K. Jha, K. Gajapure, A.L. Chakraborty, Design and evaluation of an FBG sensor-based glove to simultaneously monitor flexure of ten finger joints, IEEE Sens. J. 21 (6) (2021) 7620–7630, https://doi.org/10.1109/JSEN.2020.3046521, 2021.
[14] C.K. Jha, S. Agarwal, A.L. Chakraborty, et al., An FBG-based sensing glove to measure dynamic finger flexure with an angular resolution of 0.1° up to speeds of 80°/s, J. Lightw. Technol. 37 (18) (2019) 4734–4740, https://doi.org/10.1109/JLT.2019.2919496.
[15] L. Li, R. He, M.S. Soares, et al., Embedded FBG-based sensor for joint movement monitoring, IEEE Sens. J. 21 (2020) 26793–26798, https://doi.org/10.1109/JSEN.2021.3120995.
[16] A.B. Socorro-Leranoz, S. Diaz, S. Castillo, et al., Optical system based on multiplexed FBGs to monitor hand movements, IEEE Sens. J. 21 (13) (2021) 14081–14089, https://doi.org/10.1109/JSEN.2020.3002827.
[17] B.J. Zha, Z. Wang, L. Ma, et al., Intelligent wearable photonic sensing system for remote healthcare monitoring using stretchable elastomer optical fiber, IEEE Internet. Things. J. 11 (10) (2024) 17317–17329, https://doi.org/10.1109/JIOT.2024.3356574.
[18] N. Wang, Y. Yao, P. Wu, et al., Soft polymer optical fiber sensors for intelligent recognition of elastomer deformations and wearable applications, Sensors 24 (7) (2024) 2253, https://doi.org/10.3390/s24072253.
[19] J. Li, B. Liu, Y. Hu, et al., Plastic-optical-fiber-enabled smart glove for machine-learning-based gesture recognition, IEEE Trans. Ind. Electron. 71 (4) (2024) 4252–4261, https://doi.org/10.1109/TIE.2023.3277119.
[20] J. Zhang, X. Wang, H. Bi, et al., High-precision dynamic gesture recognition based on microfiber sensor and EMT-net, Sens. Actuators A: Phys. 379 (2024) 115852, https://doi.org/10.1016/j.sna.2024.115852.
[21] S.P. Wang, X.Y. Wang, S. Wang, et al., Optical-nanofiber-enabled gesture-recognition wristband for human-machine interaction with the assistance of machine learning, Adv. Intell. Syst. 5 (7) (2023) 2200412, https://doi.org/10.1002/aisy.202200412.
[22] X. Liang, Y. Long, K. Xiang, et al., Advancing human-computer interaction: smartphone-integrated POF speckle sensor for gesture and identity recognition, IEEe Sens. J. 24 (19) (2024) 30028–30037, https://doi.org/10.1109/JSEN.2024.3437763.
[23] Y. Guo, J. Zhang, X. Li, et al., Finger motion detection based on optical fiber Bragg grating with polyimide substrate, Sens. Actuators A: Physol. 338 (2022) 113482, https://doi.org/10.1016/j.sna.2022.113482.
[24] X. Li, Y. Guo, J. Zhang, Investigation of gesture recognition based on optical fiber Bragg grating sensors, Measurement 209 (2023) 112498, https://doi.org/10.1016/j.measurement.2023.112498.
[25] P. Yi, B. Luo, D.C. Wu, et al., Design and gesture recognition of wrist joint posture sensor based on fiber bragg gratings, IEEe Sens. J. 24 (23) (2024) 39050–39058, https://doi.org/10.1109/JSEN.2024.3481013.
[26] C. Broadway, R. Min, A.G. Leal-Junior, et al., Toward commercial polymer fiber Bragg grating sensors: review and applications, J. Lightw. Technol. 37 (11) (2019) 2605–2615, https://doi.org/10.1109/JLT.2018.2885957.
[27] H. Qu, W. Liang, X. Cheng, et al., Embedded POFBG for Respiratory and heart rate measurement, IEEE Sens. J. 25 (3) (2025) 4612–4619, https://doi.org/10.1109/JSEN.2024.3515210.
[28] Z. Wang, M. Zhang, H. Chen, et al., A generalized fault diagnosis framework for rotating machinery based on phase entropy, Reliab. Eng. Syst. Saf. 256 (2025) 110745, https://doi.org/10.1016/j.ress.2024.110745.
[29] Z. Wang, P. Liang, R. Bai, et al., Few-shot fault diagnosis for machinery using multi-scale perception multi-level feature fusion image quadrant entropy, Adv. Eng. Inform. 63 (2025) 102972, https://doi.org/10.1016/j.aei.2024.102972.
[30] Z. Wang, Y. Liu, R. Bai, et al., Multi-modal multi-scale multi-level fusion quadrant entropy for mechanical fault diagnosis, Expert. Syst. Appl. 281 (2025) 127715, https://doi.org/10.1016/j.eswa.2025.127715.
[31] K. Xiao, Z. Wang, Y.D. Ye, et al., PDMS-embedded wearable FBG sensors for gesture recognition and communication assistance, Biomed. Opt. Express. 15 (3) (2024) 1892, https://doi.org/10.1364/BOE.517104.
[32] G. Woyessa, A. Fasano, A. Stefani, et al., Single mode step-index polymer optical fiber for humidity insensitive high temperature fiber Bragg grating sensors, Opt. Express 24 (2) (2016) 1253, https://doi.org/10.1364/OE.24.001253.
[33] X. Hu, Y. Chen, S. Gao, et al., Direct bragg grating inscription in single-mode step-index TOPAS/ZEONEX polymer optical fiber using 520 nm femtosecond pulses, Polymers 14 (13) (2022) 2640, https://doi.org/10.3390/polym14132640.
[34] S.H. Jeong, S. Zhang, K. Hjort, et al., Stretchable electronic devices: pDMS-based elastomer tuned soft, stretchable, and sticky for epidermal electronics, Adv. Mater. 28 (28) (2016) 5765–5775, https://doi.org/10.1002/adma.20167019.
[35] Q. Li, R. Li, Myoelectric human-computer interaction using CNN-LSTM neural network for dynamic hand gesture recognition, J. Intell. Fuzzy Syst. 44 (3) (2023) 4207–4221, https://doi.org/10.3233/JIFS-222985.
[36] A. Filipowska, W. Filipowski, P. Raif, et al., Machine learning-based gesture recognition glove: design and implementation, Sensors 24 (18) (2024) 6157, https://doi.org/10.3390/s24186157.